Roles of Leu249, Lys252, and Leu253 in Membrane Segment M3 of Sarcoplasmic Reticulum Ca^{2+}-ATPase in Control of Ca^{2+} Migration and Long-Range Intramolecular Communication†

Johannes D. Clausen and Jens Peter Andersen*

Department of Physiology, University of Aarhus, DK-8000 Aarhus C, Denmark

Received November 18, 2002; Revised Manuscript Received January 13, 2003

ABSTRACT: Point mutants with alterations to Leu249, Lys252, Leu253, Asp254, and Glu255 in membrane segment M3, and Pro824, Lys825, and Glu826 in loop L6−7, of the sarcoplasmic reticulum Ca^{2+}-ATPase were analyzed functionally by steady-state and transient kinetic methods. In mutants Leu249Ala, Lys252Glu, and Leu253Ala, the rate of Ca^{2+} dissociation from the cytoplasmically facing high-affinity Ca^{2+} sites was increased 4- to 7-fold relative to wild type, and in Leu249Ala and Lys252Glu the rate of Ca^{2+} binding was increased as well. Substitution of Lys252 with arginine, alanine, glutamine, or methionine affected Ca^{2+} interaction much less, indicating that the negative charge of the glutamate is particularly disturbing. These findings may be understood on the basis of the hypothesis that a water-accessible channel leading between membrane segments M1 and M3 in the thapsigargin-bound Ca^{2+}-free structure [Toyoshima, C., and Nomura, H. (2002) *Nature 418*, 605−611] is closely related to the migration pathway for Ca^{2+}. The effects of alanine mutations to Leu249 and Leu253 on Ca^{2+} dissociation may arise from destabilization of the hydrophobic wall lining the pathway. In mutant Lys252Glu, unfavorable interaction between the glutamate and L6−7 may open the pathway. In addition, Leu253Ala, and to a lesser extent some of the other mutations, reduced the rate of the E_1PCa_2 to E_2P transition of the phosphoenzyme, enhanced the rate of dephosphorylation of E_2P, and reduced the apparent affinity for vanadate, suggesting interference with the conformational change of the phosphoenzyme and the function of the catalytic site in E_2 and E_2P.

The Ca^{2+}-ATPase[1] of sarcoplasmic reticulum is an ion pump that mediates the uptake of Ca^{2+} from the cytoplasm at the expense of ATP being hydrolyzed (*1*−*3*). This integral membrane protein consists of 10 membrane-spanning segments, M1−M10, of which M4, M5, M6, and M8 contribute ligands to Ca^{2+} binding, and a cytoplasmic part comprised mainly of three distinct domains named "N" for nucleotide-binding, "P" for phosphorylation, and "A" for "actuator" (*4*). During the enzyme cycle (Scheme 1), the aspartic acid residue Asp351 in domain P undergoes phosphorylation and dephosphorylation, and a crucial question is how these events are coupled with the translocation of Ca^{2+} occurring in the membrane domain some 40 Å away. The functional communication over this distance seems to be mediated by distinct conformational changes in the protein that are still poorly understood. Another important challenge to our understanding is presented by the pathway for the initial migration of the Ca^{2+} ions from the cytoplasm to the intramembranous binding sites and the mechanism responsible for the opening and closure of this pathway. The high-resolution crystal structure of the Ca^{2+}-ATPase in the Ca^{2+}-bound E_1Ca_2 form does not reveal any entry pathway for Ca^{2+} (*4*), presumably because it closes following the binding of the Ca^{2+} ions ("occlusion"). Membrane segment M3 is interesting, as it seems to occupy a rather strategic position. M3 is directly linked through the peptide backbone to the

Scheme 1: Reaction Cycle of Ca^{2+}-ATPase[a]

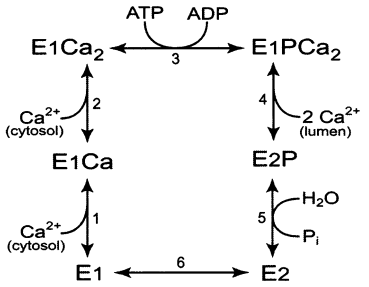

[a] The forward direction of the cycle is clockwise. At least four major conformational states are involved in the transport process, E_1, E_2, E_1P, and E_2P. In addition, the sequential binding of the two Ca^{2+} to E_1 is accompanied by further conformational rearrangements that allow E_1Ca_2 to be phosphorylated from ATP. The partial reaction steps are numbered for reference in the text and figure legends.

† This work was supported by grants from the Danish Medical Research Council, the Lundbeck Foundation, the Novo Nordisk Foundation, and the Research Foundation of Aarhus University.

* To whom correspondence should be addressed: Jens Peter Andersen, Department of Physiology, University of Aarhus, Ole Worms Allé 160, DK-8000 Aarhus C, Denmark. Fax: +45 86129065. E-mail: jpa@fi.au.dk.

[1] Abbreviations: Ca^{2+}-ATPase, the sarco(endo)plasmic reticulum Ca^{2+}-transporting adenosine triphosphatase (EC 3.6.1.38); $K_{0.5}$, ligand concentration giving half-maximum effect; L6−7, cytoplasmic loop connecting membrane-spanning segments 6 and 7; M1−M10, membrane-spanning segments; MES, 2-[*N*-morpholino]ethanesulfonic acid; MOPS, 3-[*N*-morpholino]propanesulfonic acid; TES, *N*-[tris(hydroxymethyl)-methyl]-2-aminoethane-sulfonic acid.

10.1021/bi0271897 CCC: $25.00
Published on Web 02/13/2003

actuator domain, and, furthermore, M3 participates in a hydrogen bond network with domain P and the cytoplasmic loop extending between membrane segments M6 and M7 (loop "L6−7"). The actuator domain and L6−7 have both been implicated together with domain P in the transport associated conformational rearrangements (*5*−*10*). M3 residues also participate in the binding of thapsigargin (*11*, *12*), an inhibitor that interferes both with Ca^{2+} binding and the function of the catalytic site. Furthermore, in the recently published crystal structure of the thapsigargin-bound Ca^{2+}-free form of the Ca^{2+}-ATPase, a water-accessible pocket, or channel, has opened up between M1 and M3 (*12*). This channel might provide a passage for Ca^{2+} to the binding sites in the native Ca^{2+}-free enzyme (*12*).

Information about structure−function relationships can be obtained by examining the functional consequences of site mutations, but few mutagenesis studies of the Ca^{2+}-ATPase have focused on M3. In a recent study from this laboratory (*13*), we analyzed chimeras with short sequences of the Ca^{2+}-ATPase replaced by the corresponding segments of the closely related Na^+,K^+-ATPase and found that replacement of the segment Lys252−Leu−Asp−Glu255 near the cytoplasmic end of M3 with the Na^+,K^+-ATPase segment, Glu−Ile−Glu−His, led to functional changes suggesting that this region plays previously unrecognized roles in control of Ca^{2+} migration to and from the binding sites and in the conformational changes involved in Ca^{2+} translocation (*13*). A major concern in such studies of chimeras/cluster mutants is, however, whether the observed effects can be associated to particular functionally important residues, or the effects are more unspecific, requiring the simultaneous replacement of several residues. For these reasons, we have now undertaken a more detailed study of the functional consequences of point mutations to the same residues and others in their vicinity. Interestingly, the E_1Ca_2 crystal structure shows that the side chain of Lys252 is within hydrogen bonding distance of the two backbone carbonyls of Pro824 and Glu826 in the C-terminal part of loop L6−7 (*4*), whereas in the crystal structure of the thapsigargin-bound Ca^{2+}-free form, the side chain of Lys252 has moved away from L6−7 (*12*). To investigate the importance of the interaction between Lys252 and L6−7 in E_1Ca_2, we have studied a series of point mutations with alterations to Lys252, Pro824, Lys825, and Glu826. We have, furthermore, focused our attention on the acidic residues Asp254 and Glu255, and the hydrophobic residue Leu253, which like Lys252 are part of the Lys252−Leu−Asp−Glu255 segment pinpointed in the previous study (*13*). Moreover, we have investigated the importance of Leu249, which is located one α-helical turn above Leu253 in M3. Our results demonstrate that either of the point mutations Leu249Ala, Lys252Glu, and Leu253Ala interferes profoundly with Ca^{2+} migration, and in addition Leu253 is very important for the E_1PCa_2 to E_2P transition and for the function of the catalytic site in E_2 and E_2P.

EXPERIMENTAL PROCEDURES

Mutagenesis, Expression, and Assays of Overall Function. Oligonucleotide-directed mutagenesis of cDNA encoding the rabbit fast twitch muscle Ca^{2+}-ATPase (SERCA1a isoform) was carried out as described previously (*14*). For expression, the wild-type or mutant cDNA, inserted in the pMT2 vector (*15*), was transfected into COS-1 cells (*16*) using the calcium phosphate precipitation method (*17*). The microsomal fraction containing expressed wild-type or mutant Ca^{2+}-ATPase was isolated by differential centrifugation (*18*). The concentration of expressed wild type or mutant was quantified by a specific enzyme-linked immunosorbent assay (*19*), using as standard expressed wild-type SERCA1a, for which the concentration had been determined by measurement of the maximum capacity for phosphorylation by inorganic phosphate in the presence of 30% (v/v) dimethyl sulfoxide (*20*). In some cases, the determination of maximum capacity for phosphorylation was, furthermore, used as an additional assay to check the concentration of expressed mutant Ca^{2+}-ATPase. The ATP-driven transport of $^{45}Ca^{2+}$ into the microsomal vesicles was measured by filtration, and the ATPase activity by determining the amount of P_i liberated (*20*, *21*) under conditions corresponding to maximal activity for the wild type at 37 °C, pH 7.0, and 5 mM MgATP. Following subtraction of the background activity determined with control microsomes isolated from mock-transfected COS-1 cells, the specific activity ("turnover rate") was calculated by relating the rate of Ca^{2+} transport or ATP hydrolysis to the expression level.

Phosphorylation from [γ-^{32}P]ATP and $^{32}P_i$. Manual mixing experiments at various buffer and temperature conditions (detailed in the figure legends) were carried out according to the principles described previously (*5*, *14*, *19*, *20*). Transient kinetic experiments at 25 °C were performed using a Bio-Logic quench-flow module QFM-5, as described (*22*), or using a Bio-Logic quench-flow module SFM-400/Q (Bio-Logic Science Instruments, Claix, France) that works by the same principle as the QFM-5 module. Even though the two quench-flow modules gave essentially identical results, each set of experiments was performed exclusively on the same module. Acid quenching of phosphorylated enzyme was performed with 0.5−2 volumes of 25% (w/v) trichloroacetic acid containing 100 mM H_3PO_4. The acid-precipitated protein was washed by centrifugation and subjected to SDS−polyacrylamide gel electrophoresis in a 7% polyacrylamide gel at pH 6.0 (*5*), and the radioactivity associated with the separated Ca^{2+}-ATPase band was quantified by imaging, using a Packard Cyclone Storage Phosphor system. Background phosphorylation levels were subtracted from all data points. The background was determined in parallel experiments, either with control microsomes isolated from mock-transfected COS-1 cells or by adding an excess of EGTA to remove Ca^{2+} before initiating the phosphorylation. In some of the dephosphorylation experiments, the constant phosphorylation level reached after the exponential decay was taken as background.

Calculations and Data Analysis. The SigmaPlot program (SPSS Inc.) was used to analyze the data by nonlinear regression, and the best fits are shown as lines in the figures. Extracted parameters are given in the tables and figure legends. The analysis of ligand concentration dependences was based on the Hill function. Monoexponential functions were fitted to the phosphorylation and dephosphorylation time courses. Generally, the experiments were conducted at least twice. Standard errors are indicated for the means and for parameters extracted by regression analysis in those cases where the analysis was based on $n \geq 4$ determinations.

Table 1: Results of the Functional Analysis of Overall and Partial Reactions

mutation	max turnover rate[a] (s^{-1})	turnover rate in the absence of ionophore[b] (%)	Ca^{2+} transport[c] (%)	$K_{0.5}$ for Ca^{2+} activation of ATPase activity[d] (μM)	rate of Ca^{2+} dissociation[e] (s^{-1})	rate of Ca^{2+} binding[f] (s^{-1})	$K_{0.5}$ for vanadate inhibition[g] (μM)	rate of dephosphorylation of E_1PCa_2[h] (min^{-1})	rate of dephosphorylation of E_2P[i] (min^{-1})
wild type	117 ± 2[j]	41 ± 1.3	100 ± 2	0.31 ± 0.01	2.2 ± 0.1	20.9 ± 0.9	0.17 ± 0.01	19.1 ± 1.1	2.1 ± 0.1
Leu249Ala	111 ± 3	37	107 ± 3	0.32 ± 0.01	11.1 ± 0.9	27.5 ± 1.2	0.93 ± 0.08	17.8 ± 1.9	7.0 ± 1.1
Lys252Ala	106	35	108 ± 9	0.36 ± 0.02	3.2 ± 0.2	25.5 ± 1.8	0.16 ± 0.02	22.1 ± 1.9	5.2 ± 0.3
Lys252Glu	91 ± 6	32	86 ± 6	0.37 ± 0.01	8.9 ± 0.3	54.1 ± 2.1	1.24 ± 0.13	12.2 ± 1.2	8.0 ± 0.3
Lys252Gln	113 ± 6	34	97 ± 10	0.35 ± 0.02	3.3 ± 0.1	31.8 ± 3.0	0.15 ± 0.02	19.7 ± 2.0	6.3 ± 0.4
Lys252Met	115 ± 7	39	114 ± 17	0.37 ± 0.01	4.0 ± 0.1	29.6 ± 2.5	0.14 ± 0.01	18.0 ± 1.7	4.2 ± 0.6
Lys252Arg	106 ± 6	41	105 ± 12	0.36 ± 0.02	3.3 ± 0.1	24.3 ± 1.5	0.12 ± 0.02	18.0 ± 1.4	5.0 ± 0.4
Leu253Ala	47 ± 4	29	43 ± 6	0.20 ± 0.02	14.7 ± 1.4	20.5 ± 1.1	1.57 ± 0.20	4.5 ± 0.5	28.6 ± 1.5
Asp254Ala	70 ± 5	32	67 ± 3	0.25 ± 0.02	3.3 ± 0.2	20.9 ± 1.6	0.14 ± 0.01	7.6 ± 0.6	10.0 ± 0.8
Glu255Ala	110 ± 10	30	100 ± 6	0.31 ± 0.02	2.4 ± 0.1	23.4 ± 1.0	0.15 ± 0.01	14.2 ± 1.8	3.0 ± 0.4
Glu255His	114 ± 7	34	98	0.39 ± 0.03	3.2 ± 0.2	27.4 ± 1.5	0.19 ± 0.02	15.2 ± 1.1	3.4 ± 0.1
Pro824Leu	86 ± 7	38	105 ± 13	0.30 ± 0.01	3.2 ± 0.2	24.6 ± 1.7	0.31 ± 0.03	13.3 ± 1.0	2.8 ± 0.3
Lys825Leu	102 ± 9	51	103 ± 9	0.26 ± 0.02	3.9 ± 0.1	27.6 ± 2.3	0.14 ± 0.01	17.1 ± 1.5	2.5 ± 0.1
Glu826Leu	75 ± 6	49	95 ± 10	0.17 ± 0.01	2.6 ± 0.1	27.9 ± 1.5	0.22 ± 0.02	14.3 ± 1.6	3.8 ± 0.5

[a] The maximum rate of Ca^{2+}-activated ATP hydrolysis was determined at 37 °C in the presence of 1 μM Ca^{2+} ionophore A23187, using the Baginski method (*20*, *21*) to measure the amount of P_i liberated during a 10-min incubation of the microsomes in a medium containing 50 mM TES/Tris (pH 7.0), 100 mM KCl, 7 mM $MgCl_2$, 1 mM EGTA, 0.9 mM $CaCl_2$ (giving a free Ca^{2+} concentration of 3 μM), and 5 mM ATP. The ATPase turnover rate was calculated as the amount of P_i liberated per Ca^{2+}-ATPase molecule per second. [b] The ATPase turnover rate was determined as described above, except for the exclusion of Ca^{2+} ionophore A23187. The percentages indicate the turnover rates determined in the absence of ionophore relative to those determined in its presence. [c] Measurements of ATP-driven Ca^{2+} transport were performed by filtration following incubation for 5 min at 37 °C in a medium containing 20 mM MOPS/Tris (pH 6.8), 100 mM KCl, 5 mM MgATP, 5 mM potassium oxalate, 0.5 mM EGTA, and 0.45 mM $^{45}CaCl_2$. The Ca^{2+} transport activity of the wild type was taken as 100% and each mutant was related to this level following correction for the variation of expression level. [d] The ATPase turnover rate was determined as described above (Ca^{2+} ionophore present), but at varying concentrations of Ca^{2+}. The $K_{0.5}$ values for Ca^{2+} activation were deduced by fitting the Hill equation. [e] The rate of Ca^{2+} dissociation at 25 °C, pH 6.0 determined as described for Figure 1. [f] The rate of phosphorylation at pH 7.0, 25 °C determined following simultaneous addition of [γ-^{32}P]ATP and Ca^{2+} to Ca^{2+}-deprived enzyme as described for Figure 3 (examination of the reaction sequence consisting of reactions 6, 1, 2, and 3 in Scheme 1). [g] The apparent affinity for vanadate determined as described for Figure 5. [h] The rate of dephosphorylation of E_1PCa_2 phosphoenzyme determined at 0 °C as described for Figure 6 (examination of the $E_1PCa_2 \rightarrow E_2P$ transition, i.e., reaction 4 in Scheme 1). [i] The rate of dephosphorylation of E_2P phosphoenzyme determined as described for Figure 7 (reaction 5 in Scheme 1). [j] Standard errors are indicated in those cases where the analysis was based on $n \geq 4$ determinations.

RESULTS

Mutagenesis and Expression. The 13 point mutations to the Ca^{2+}-ATPase examined in the present study are listed in Table 1. Lys252 was replaced with alanine, glutamate (the substitution present in the Na^+,K^+-ATPase), glutamine, methionine, and arginine to study the effects of variations in size, polarity, and charge of the side chain. Residues Leu249, Leu253, and Asp254, which show a high degree of homology to the corresponding residues in the Na^+,K^+-ATPase (Ile279, Ile283, and Glu284, respectively, in the rat α_1 form), were each replaced by alanine. Glu255 was replaced with alanine or histidine, the latter being the residue found at the corresponding position in the Na^+,K^+-ATPase (i.e., His285). The interaction between the side chain of Lys252 and L6−7 was furthermore studied by replacement of Pro824, Lys825, and Glu826 with leucine. Although Lys252 is believed to interact with the main chain carbonyls of Pro824 and Glu826 (*4*), we speculated that changes to the side chains of these residues might cause some perturbation of the main chain that would interfere with the bonds to Lys252. All the mutants could be expressed in COS-1 cells to levels similar to that of the wild type.

Assays for Overall Function. To assess the overall function of the mutants, we measured the maximum rate of Ca^{2+}-activated ATP hydrolysis at 37 °C in the presence and absence of the calcium ionophore A23187 (Table 1). The ionophore permits passive efflux of Ca^{2+} accumulated in the microsomal vesicles, whereby the "back inhibition" imposed by Ca^{2+} accumulated at high concentration in the vesicles is avoided (*20*). Mutants Leu253Ala and Asp254Ala showed the most pronounced reduction of the turnover rate, to 40 and 60% of wild type, respectively. For Lys252Glu, Pro824Leu, and Glu826Leu, the turnover rate was affected to a lesser extent, and for the remaining mutants the turnover rate was indistinguishable from wild type. In the absence of calcium ionophore, the ATPase activity was 2−3-fold lower than that measured in the presence of ionophore for the wild type and all the mutants (Table 1), demonstrating that the mutants were able to pump Ca^{2+} and, like the wild type, were inhibited by luminal Ca^{2+}. The ability to transport Ca^{2+} was also demonstrated by direct measurement of the rate of $^{45}Ca^{2+}$ accumulation in the microsomal vesicles at 37 °C in the presence of oxalate to trap Ca^{2+} in the lumen (Table 1). The mutational effects on Ca^{2+} transport are seen to be similar to those described above for the rate of ATP hydrolysis, indicating a retained coupling between ATP hydrolysis and Ca^{2+} translocation in the mutants.

The turnover rate for ATP hydrolysis was furthermore measured at varying concentrations of Ca^{2+} (data not shown). The Ca^{2+} concentration giving half-maximum activation of ATP hydrolysis was deduced by fitting the Hill equation to the data, and the Ca^{2+} activation constants are listed in Table 1. A 1.5−2-fold higher apparent Ca^{2+} affinity (lower $K_{0.5}$) relative to wild type was evident for mutants Leu253Ala and Glu826Leu. For the remaining mutants, the $K_{0.5}$ values for Ca^{2+} activation deviated less or insignificantly from that of the wild type.

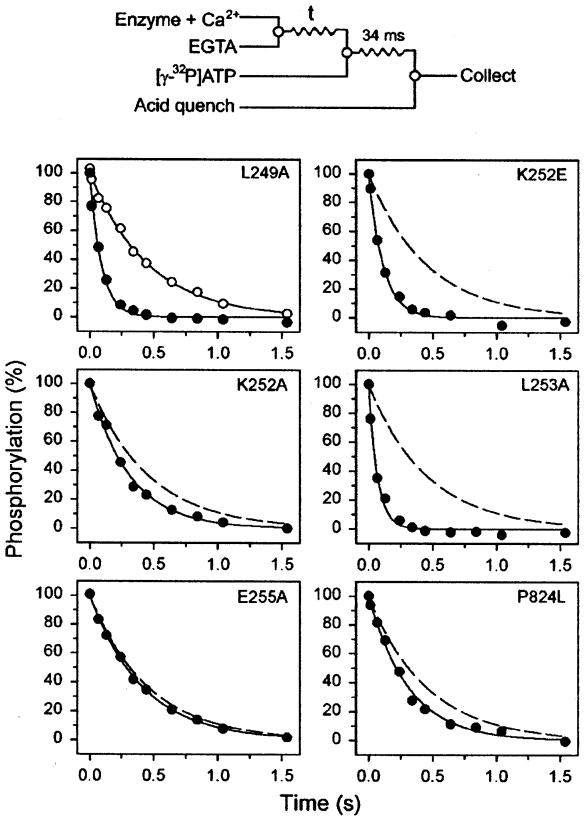

FIGURE 1: Rate of Ca^{2+} dissociation at pH 6.0: examination of reaction 2, reverse, in Scheme 1. Quench-flow experiments were carried out as illustrated in the diagram above the panels using a SFM-400/Q module at 25 °C. Wild-type (open circles) or mutant (solid circles) enzyme preincubated in medium containing 40 mM MES/Tris (pH 6.0), 80 mM KCl, 5 mM $MgCl_2$, and 100 μM $CaCl_2$ was mixed with an equal volume of 40 mM MES/Tris (pH 6.0), 80 mM KCl, 5 mM $MgCl_2$, and 4 mM EGTA. At the time interval indicated on the abscissa, the double volume of 40 mM MES/Tris (pH 6.0), 80 mM KCl, 5 mM $MgCl_2$, 2 mM EGTA, and 10 μM [γ-^{32}P]ATP was added, followed by acid quenching 34 ms later. To obtain the point corresponding to zero time, 4 mM EGTA was replaced by 100 μM $CaCl_2$. The lines show the best fit of a monoexponential decay function, giving the rate constants listed in Table 1. The broken lines correspond to the wild-type curve from the upper left panel.

Rate of Ca^{2+} Dissociation. Ca^{2+} dissociation from E_1Ca_2 was studied by the previously described rapid kinetic methods (*13*, *22*). The assays for Ca^{2+} dissociation take advantage of the fact that phosphorylation from ATP requires occupancy of the Ca^{2+} sites (*23*). When free Ca^{2+} is removed from Ca^{2+}-saturated enzyme by addition of a Ca^{2+} chelator such as EGTA, the ability to phosphorylate disappears at a rate corresponding to that of the first Ca^{2+} dissociation step in the sequential mechanism (reaction 2, reverse, in Scheme 1), because activation of phosphorylation requires the binding of both Ca^{2+} ions (*23*). The results shown in Figure 1 were obtained at 25 °C and pH 6.0 by mixing the Ca^{2+}-saturated enzyme with an excess of EGTA to allow Ca^{2+} to dissociate for the indicated time intervals, followed by testing the ability to phosphorylate by a 34-ms incubation with [γ-^{32}P]ATP prior to acid quenching, as indicated in the flow diagram at the top of the figure. As seen in Figure 1, good fits of a monoexponential decay function to the data could be obtained. The extracted rate constant for Ca^{2+} dissociation is listed in Table 1 for the wild type and all mutants. A conspicuous increase of the rate constant (4−7-fold), relative to wild type, was seen for Leu249Ala, Lys252Glu, and Leu253Ala, whereas the other mutants showed much smaller effects (up to 2-fold increase).

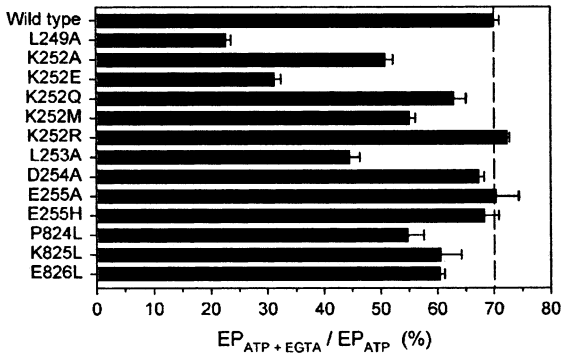

FIGURE 2: Ca^{2+} dissociation at pH 7.0: examination of reaction 2, reverse, in Scheme 1. The phosphorylation level of enzyme preincubated in medium containing 40 mM MOPS/Tris (pH 7.0), 80 mM KCl, 5 mM $MgCl_2$, and 100 μM $CaCl_2$ was determined 34 ms after mixing with an equal volume of a medium containing 40 mM MOPS/Tris (pH 7.0), 80 mM KCl, 5 mM $MgCl_2$, 10 μM [γ-^{32}P]ATP and either 4 mM EGTA ("$EP_{ATP+EGTA}$") or 100 μM $CaCl_2$ ("EP_{ATP}"), using the quench flow module QFM-5 at 25 °C as previously described (*22*). The columns show the ratio between $EP_{ATP+EGTA}$ and EP_{ATP}, which is inversely related to the rate of Ca^{2+} dissociation.

To obtain information about the mutational effects on Ca^{2+} dissociation at pH 7.0, where the rate of the wild type is considerably higher than at pH 6.0, we used the previously validated simple approach based on a single time point at 34 ms (*13*, *22*). Figure 2 shows the ratio $EP_{ATP+EGTA}/EP_{ATP}$ determined at pH 7.0. "$EP_{ATP+EGTA}$" is the amount of phosphoenzyme measured 34 ms after the simultaneous addition of [γ-^{32}P]ATP and excess EGTA to Ca^{2+}-saturated enzyme. "EP_{ATP}" is the amount of phosphoenzyme measured 34 ms after the addition of [γ-^{32}P]ATP without EGTA to Ca^{2+}-saturated enzyme, i.e., under conditions where Ca^{2+} is present in the medium. When EGTA is added together with [γ-^{32}P]ATP, the E_1Ca_2 species partitions between phosphorylation (reaction 3, forward, in Scheme 1), forming E_1PCa_2, and dissociation of the first Ca^{2+} (reaction 2, reverse, in Scheme 1), leading to the nonphosphorylatable E_1Ca intermediate. An increase of the rate of Ca^{2+} dissociation therefore reduces the $EP_{ATP+EGTA}/EP_{ATP}$ ratio. Figure 2 shows that the $EP_{ATP+EGTA}/EP_{ATP}$ ratio was markedly reduced relative to wild type for mutants Leu249Ala, Lys252Glu, and Leu253Ala (to 23, 31, and 45%, respectively, compare with 70% for wild type), consistent with an increase of the Ca^{2+} dissociation rate. Previously, we found a value of 27% for the chimeric cluster mutant in which Lys252−Leu−Asp−Glu255 had been replaced by Glu−Ile−Glu−His (*13*). As further seen in Figure 2, the conservative mutation Lys252Arg and the mutations to Asp254 and Glu255 had little or no influence on the $EP_{ATP+EGTA}/EP_{ATP}$ ratio. A reduction to values ranging between 51 and 63% was seen for the remaining Lys252 mutants and for the three L6−7 mutants.

Rates of Phosphorylation and Ca^{2+} Binding. Using the rapid quench module, the time course of phosphorylation with [γ-^{32}P]ATP was studied at pH 7.0, 25 °C, either for enzyme preincubated with a saturating Ca^{2+} concentration of 100 μM, or upon simultaneous addition of [γ-^{32}P]ATP with Ca^{2+} (giving a final free Ca^{2+} concentration of 100 μM)

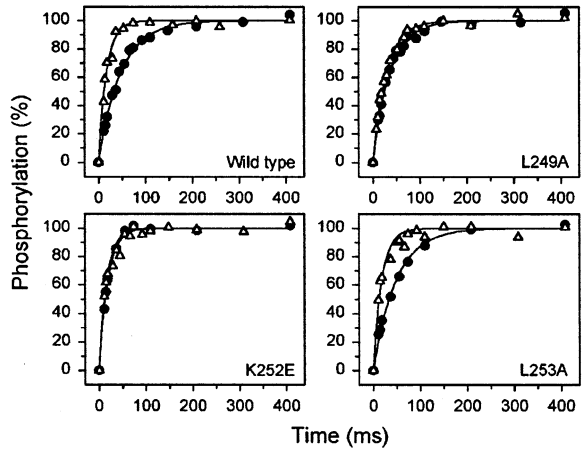

FIGURE 3: Time course of phosphorylation from [γ-^{32}P]ATP at 25 °C and pH 7.0 of enzyme preincubated in the presence of Ca^{2+} (examination of reaction 3 in Scheme 1) or absence of Ca^{2+} (examination of the reaction sequence consisting of reactions 6, 1, 2, and 3 in Scheme 1). The experiments were carried out using a QFM-5 quench-flow module at 25 °C with mixing protocols as previously described (*22*). To monitor the phosphorylation of enzyme initially present in the Ca^{2+}-bound form (open triangles), microsomes suspended in a buffer containing 40 mM MOPS/Tris (pH 7.0), 80 mM KCl, 100 μM $CaCl_2$, and 5 mM $MgCl_2$ were mixed with an equal amount of the same buffer containing in addition 10 μM [γ-^{32}P]ATP, followed by acid quenching at the indicated time intervals. To monitor the phosphorylation of enzyme initially present in the Ca^{2+}-deprived form (solid circles), microsomes suspended in a buffer containing 40 mM MOPS/Tris (pH 7.0), 80 mM KCl, and 2 mM EGTA were mixed with an equal amount of buffer containing 40 mM MOPS/Tris (pH 7.0), 80 mM KCl, 2.2 mM $CaCl_2$, 10 mM $MgCl_2$, and 10 μM [γ-^{32}P]ATP, followed by acid quenching at the indicated time intervals. In each case, the maximal level of phosphorylation was taken as 100%. The lines show the best fits of a monoexponential function. The respective rate constants obtained following preincubation in the presence and absence of Ca^{2+} are as follows: wild type, 57.6 $\pm$ 2.0 s^{-1}, 20.9 $\pm$ 0.9 s^{-1}; Leu249Ala, 33.9 $\pm$ 1.5 s^{-1}, 27.5 $\pm$ 1.2 s^{-1}; Lys252Glu, 59.3 $\pm$ 3.4 s^{-1}, 54.1 $\pm$ 2.1 s^{-1}; Leu253Ala, 54.8 $\pm$ 4.0 s^{-1}, 20.5 $\pm$ 1.1 s^{-1}.

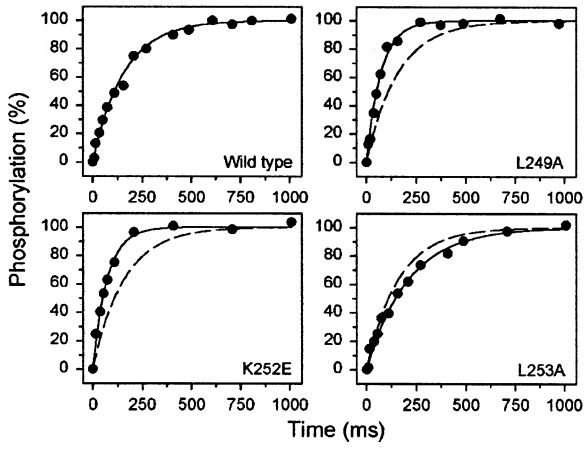

FIGURE 4: Time course of phosphorylation from [γ-^{32}P]ATP at 25 °C and pH 6.0 of enzyme preincubated in absence of Ca^{2+}: Examination of the proton dissociation steps associated with reactions 6 and 1 in Scheme 1. The experiments were carried out as for Figure 3, enzyme initially present in the Ca^{2+}-deprived form, except that 40 mM MES/Tris (pH 6.0) was used as buffer instead of MOPS/Tris. The lines show the best fits of a monoexponential function, giving the following rate constants: wild type, 6.3 $\pm$ 0.3 s^{-1}; Leu249Ala, 13.7 $\pm$ 0.9 s^{-1}; Lys252Glu, 13.7 $\pm$ 0.7 s^{-1}; Leu253Ala, 4.8 $\pm$ 0.3 s^{-1}. The broken lines correspond to the wild-type curve from the upper left panel.

to enzyme preincubated in the absence of Ca^{2+}. In the wild type, phosphorylation is slower in the latter condition than in the former, because in addition to reaction 3 of Scheme 1, also Ca^{2+} binding with associated conformational changes (the Ca^{2+} binding $E_2 \rightarrow E_1Ca_2$ transition, cf. Scheme 1, reactions 6, 1, and 2) contribute to rate limitation. Figure 3 shows the data for selected mutants, and Table 1 lists for all the mutants the rate constant for phosphorylation determined following preincubation in the absence of Ca^{2+} ("rate of Ca^{2+} binding"). This rate constant was slightly increased, relative to wild type, in several of the mutants. However, for mutant Lys252Glu a conspicuous increase of the rate constant, to 54 s^{-1}, was seen. This value is indistinguishable from that of 59 s^{-1} obtained following preincubation in the presence of Ca^{2+} (i.e., corresponding to $E_1Ca_2 \rightarrow E_1PCa_2$, cf. Scheme 1, reaction 3), the two curves being superimposable (Figure 3). Hence, in Lys252Glu, the phosphorylation rate determined following preincubation in the absence of Ca^{2+} seems to be limited only by the $E_1Ca_2 \rightarrow E_1PCa_2$ step (reaction 3) and not by the Ca^{2+} binding transition, $E_2 \rightarrow E_1Ca_2$ (reactions 6, 1, and 2 in Scheme 1), indicating that the rate of $E_2 \rightarrow E_1Ca_2$ (the "on-rate" for Ca^{2+}) is markedly enhanced in Lys252Glu, relative to wild type. A similar reasoning holds for mutant Leu249Ala, because in this mutant, as well, the observed rate constant was almost the same following preincubation in the absence and presence of Ca^{2+} (28 and 34 s^{-1}, respectively, Figure 3). None of the other mutants, including Leu253Ala (Figure 3), showed such a coalescence of the rate constants observed following preincubation in the absence and presence of Ca^{2+}.

For the wild type and mutants Leu249Ala, Lys252Glu, and Leu253Ala, the rate of phosphorylation of enzyme preincubated in the absence of Ca^{2+} was, furthermore, studied at pH 6.0, where the ion binding sites of the E_2 form are thought to be protonated, so that proton dissociation ("deocclusion"), occurring in relation to reactions 6 and 1 of Scheme 1, contributes to rate limitation of the $E_2 \rightarrow E_1Ca_2$ transition (*24*). Under these conditions, the respective rate constants were 6.3, 13.7, 13.7, and 4.8 s^{-1} (Figure 4). The enhancement of the $E_2 \rightarrow E_1Ca_2$ transition at pH 6.0 seen for Leu249Ala and Lys252Glu is in line with the above-described finding for these mutants at pH 7.0 and suggests that in addition to Ca^{2+} binding and dissociation, proton dissociation is accelerated relative to wild type.

Vanadate Binding. To further study the equilibrium between E_2 and E_1 (reaction 6 in Scheme 1) and the vanadate binding properties of the E_2 form, we determined the apparent affinity for vanadate (Figure 5). Vanadate is believed to act as a transition state analogue of the phosphoryl group (*25*) and binds preferentially to the E_2 form, thereby arresting the Ca^{2+}-ATPase in a stable E_2−vanadate complex (*26*). Following equilibration with various concentrations of vanadate in the absence of Ca^{2+} and ATP, the amount of phosphoenzyme formed upon the addition of Ca^{2+} and [γ-^{32}P]ATP was measured. Vanadate binding is competitive with respect to phosphorylation, and because the dissociation of vanadate is very slow at 0 °C (half-life for the enzyme-vanadate complex of the order of hours both for wild type and mutants), the amount of phosphoenzyme formed in this assay reflects the equilibrium between the free and vanadate-bound enzyme forms existing before the addition of Ca^{2+} and

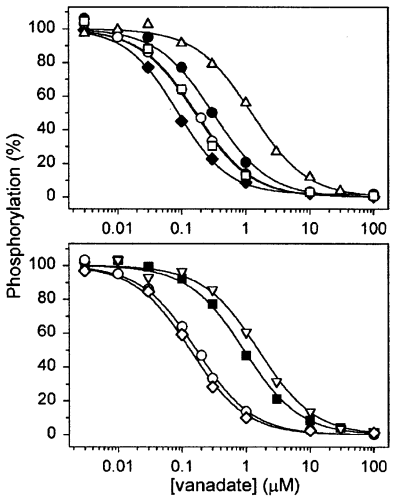

FIGURE 5: Vanadate inhibition of phosphorylation: examination of the equilibrium between E_2 and E_1 (reaction 6 in Scheme 1) and the vanadate binding properties of the E_2 form. Microsomes were incubated for 1 h at 25 °C and subsequently 15 min at 0 °C in a buffer containing 40 mM MOPS/Tris pH 7.0, 80 mM KCl, 5 mM $MgCl_2$, 2 mM EGTA, and the indicated concentrations of orthovanadate. Phosphorylation was then carried out by sequential addition of 2.5 mM $CaCl_2$ and 5 μM [γ-^{32}P]ATP at 0 °C, followed by acid quenching 15 s later. The maximal level of phosphorylation obtained in the absence of vanadate was taken as 100%. The lines show the best fits of the equation $EP = EP_{max}(1 - [\text{vanadate}]/(K_{0.5} + [\text{vanadate}]))$, giving the $K_{0.5}$ values listed in Table 1. Open circles, wild type; open squares, Lys252Ala; triangles pointing upward, Lys252Glu; solid circles, Pro824Leu; solid diamonds, Lys758Ile; solid squares, Leu249Ala; triangles pointing downward, Leu253Ala; open diamonds, Asp254Ala. Mutant Lys758Ile ($K_{0.5} = 86 \pm 4$ nM) described previously (*20*) was included for comparison.

[γ-^{32}P]ATP. From the results shown in Figure 5, it is clear that mutants Leu249Ala, Lys252Glu, and Leu253Ala all displayed much lower apparent affinity for vanadate (5-, 7-, and 9-fold, respectively) than the wild type, whereas for the remaining mutants the apparent affinity for vanadate differed much less or insignificantly from that of the wild type (Figure 5 and Table 1). The reduced apparent affinity for vanadate may reflect either a depletion of the vanadate-reactive E_2 state or a reduction of the "true" affinity of E_2 for vanadate (destabilization of the E_2−vanadate complex). For comparison, results obtained with mutant Lys758Ile were included in Figure 5 to exemplify a mutant with a reduced rate of the $E_2 \rightarrow E_1Ca_2$ transition (*20*). Lys758Ile displayed a 2-fold increased apparent affinity for vanadate, relative to wild type, consistent with accumulation of E_2.

The E_1PCa_2 to E_2P Conformational Transition. The decay of phosphoenzyme was examined following phosphorylation with [γ-^{32}P]ATP under conditions known for the wild type to lead to accumulation of the E_1PCa_2 intermediate (0 °C, neutral pH, presence of K^+). This intermediate can dephosphorylate either in the backward direction of the reaction cycle by transfer of the phosphoryl group to ADP, yielding ATP (reaction 3, reverse, in Scheme 1), or in the forward direction via the $E_1PCa_2 \rightarrow E_2P$ conversion (reaction 4, forward, in Scheme 1) followed by E_2P hydrolysis (reaction 5, forward, in Scheme 1). A chase with 1 mM ADP resulted in a very rapid dephosphorylation of the mutants, indistinguishable from that of the wild type (less than 5% of the initial phosphoenzyme remaining after 5 s dephosphorylation, data not shown), demonstrating that for the mutants, as for the wild type, the phosphoenzyme was initially present in the ADP-sensitive E_1PCa_2 form. When on the other hand the dephosphorylation in the forward direction was examined by chase with 0.6 mM nonradioactive ATP, the decay rate was for some of the mutants significantly lower than that of the wild type (Figure 6 and Table 1). Leu253Ala showed a pronounced reduction of the dephosphorylation rate to 24% of wild type. Also mutants Asp254Ala and Lys252Glu showed significant reductions of the dephosphorylation rate, to 40 and 64% of wild type, respectively, whereas the other four Lys252 mutants were indistinguishable from wild type. Some of the remaining mutants, including Pro824Leu and Glu826Leu that displayed a slightly reduced rate of ATP hydrolysis, also showed a slight reduction of the dephosphorylation rate, relative to wild type (Table 1). The reaction sequence studied here comprises the conformational transition $E_1PCa_2 \rightarrow E_2P$ (reaction 4, forward, in Scheme 1) followed by the hydrolysis of the E_2P phosphoenzyme (reaction 5, forward, in Scheme 1). It is well-known that for wild type the latter step is much faster than the former under the experimental conditions corresponding to Figure 6. As will be demonstrated in the following paragraph, none of the mutations reduced the rate of E_2P hydrolysis, implying that the step limiting the dephosphorylation rate was the $E_1PCa_2 \rightarrow E_2P$ transition (reaction 4, forward, in Scheme 1).

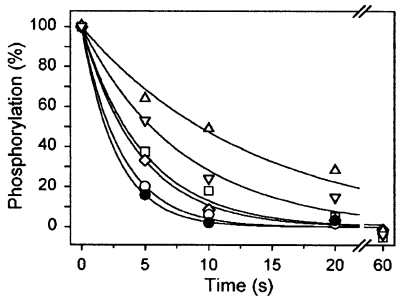

FIGURE 6: Dephosphorylation at 0 °C of E_1PCa_2 phosphoenzyme formed from [γ-^{32}P]ATP: Examination of the $E_1PCa_2 \rightarrow E_2P$ transition (reaction 4 in Scheme 1). Phosphorylation was performed for 15 s at 0 °C in a medium containing 40 mM MOPS/Tris (pH 7.0), 80 mM KCl, 5 mM $MgCl_2$, 1 mM EGTA, 0.955 mM $CaCl_2$ (giving a free Ca^{2+} concentration of 10 μM), 10 μM calcium ionophore A23187, and 5 μM [γ-^{32}P]ATP. To monitor the dephosphorylation, the phosphoenzyme was chased by addition of 600 μM nonradioactive ATP, and acid quenching was performed at the indicated time intervals. The lines show the best fit of a monoexponential decay function, giving the rate constants listed in Table 1. Open circles, wild type; solid circles, Lys252Ala; squares, Lys252Glu; triangles pointing upward, Leu253Ala; triangles pointing downward, Asp254Ala; diamonds, Pro824Leu.

Dephosphorylation of E_2P. The Ca^{2+}-ATPase in the Ca^{2+}-free E_2 form can be phosphorylated in the backward direction of normal turnover by inorganic phosphate (reaction 5, reverse, in Scheme 1). This reaction requires Mg^{2+} and is promoted by acid pH and presence of the organic solvent dimethyl sulfoxide (*27*). The phosphorylation level reached by incubation with $^{32}P_i$ under optimal conditions for E_2P formation was for all mutants indistinguishable from that of the wild type (i.e., >90%, data not shown). To study the rate of dephosphorylation of the E_2P phosphoenzyme (reaction 5, forward, in Scheme 1), the phosphorylated enzyme was diluted into a medium of the same composition except for the absence of radioactive phosphate, a reduction of the dimethyl sulfoxide concentration from 30 to 15%, and the

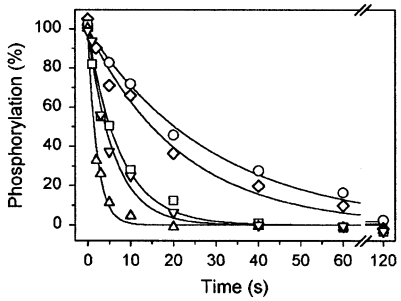

FIGURE 7: Dephosphorylation of phosphoenzyme formed from $^{32}P_i$: Examination of E_2P hydrolysis (reaction 5 in Scheme 1). Wild type and mutants were phosphorylated at 25 °C for 10 min in a medium containing 100 mM MES/Tris (pH 6.0), 2 mM EGTA, 30% (v/v) dimethyl sulfoxide, 10 mM $MgCl_2$, and 0.5 mM $^{32}P_i$. Dephosphorylation was studied at 25 °C by a 19-fold dilution into a medium containing EDTA (to remove free Mg^{2+}) corresponding to a final concentration of 10 mM, 100 mM MES/Tris (pH 6.0), 2 mM EGTA, 15% (v/v) dimethyl sulfoxide, and 0.5 mM nonradioactive P_i, followed by acid quenching at serial time intervals. The lines show the best fit of a monoexponential decay function, giving the rate constants listed in Table 1. Circles, wild type; squares, Lys252Glu; triangles pointing upward, Leu253Ala; triangles pointing downward, Asp254Ala; diamonds, Pro824Leu.

presence of an excess of EDTA to remove Mg^{2+} and, thus, terminate phosphorylation. As seen in Figure 7 and Table1, several mutants showed a markedly increased rate of E_2P hydrolysis relative to wild type, most pronounced for Leu253Ala (14-fold), Asp254Ala (5-fold), and Lys252Glu (4-fold).

Ca^{2+} Dependence of Steady-State Phosphorylation. Figure 8 and Table 2 show the results of titrating the Ca^{2+} dependence of steady-state phosphorylation from [γ-^{32}P]ATP for selected mutants. At 25 °C, the $K_{0.5}$ for Ca^{2+} activation of mutants Leu249Ala, Lys252Glu, and Lys252Arg was indistinguishable from that of the wild type, whereas the $K_{0.5}$ for Leu253Ala was slightly reduced (corresponding to an increased apparent affinity), consistent with the result obtained by Ca^{2+} titration of the ATPase activity (Table 1). Given that the Ca^{2+} dissociation rate ("off-rate" for Ca^{2+}) was increased in Leu249Ala, Lys252Glu, and Leu253Ala, relative to wild type (Figures 1 and 2), a reduction of apparent affinity for Ca^{2+} might have been expected. For Leu249Ala and Lys252Glu, the normal apparent affinity for Ca^{2+} may, however, be ascribed to the increase of the on-rate for Ca^{2+} (Figures 3 and 4), balancing the increased off-rate. For Leu253Ala, there was no indication of an increased on-rate (Figures 3 and 4), but the rate of the $E_1PCa_2 \rightarrow E_2P$ transition was reduced considerably (Figure 6). As previously demonstrated by computer simulation (*13*), a change of $K_{0.5}$ for Ca^{2+} activation of phosphorylation at steady-state toward lower values (increase of apparent affinity) should indeed be expected when phosphoenzyme turnover is reduced, because lower Ca^{2+} concentrations are required for the phosphoenzyme to accumulate under these conditions.

It should, furthermore, be noticed that for Leu249Ala, Lys252Glu, and Leu253Ala, the Ca^{2+} activation profile showed a tendency to be steeper than the activation profiles corresponding to the wild type and mutant Lys252Arg (Figure 8). The steepness of the curves can be evaluated quantitatively by comparing the Hill numbers (n_H values in Table 2) extracted by fitting the Hill equation to the data, and a slight increase of the n_H value relative to wild type

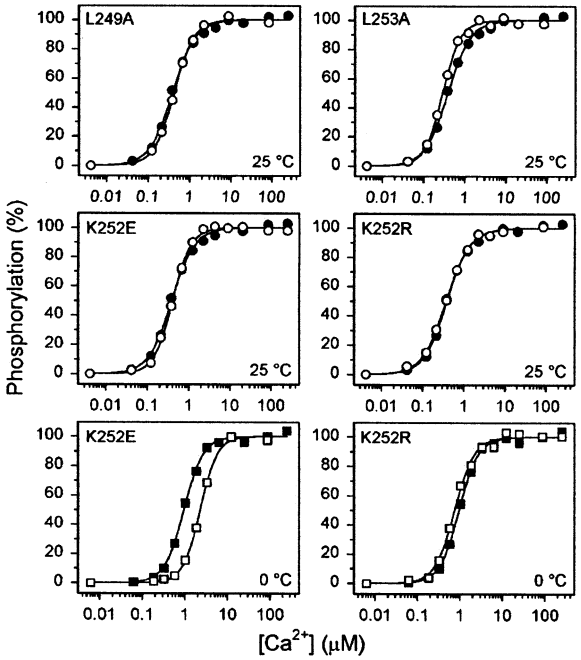

FIGURE 8: Ca^{2+} dependence of steady-state phosphorylation from [γ-^{32}P]ATP. Phosphorylation was performed with wild type (solid symbols) and selected mutants (open symbols) by manual mixing, either for 5 s at 25 °C (circles) or for 15 s at 0 °C (squares) in a medium containing 40 mM MOPS/Tris (pH 7.0), 80 mM KCl, 5 mM $MgCl_2$, 1 mM EGTA, 5 μM [γ-^{32}P]ATP, and varying concentrations of $CaCl_2$ to set the free Ca^{2+} concentration as indicated. The lines show the best fits of the Hill equation, $EP = EP_{max}[Ca^{2+}]^n/(K_{0.5}^n + [Ca^{2+}]^n)$, to the data, giving the $K_{0.5}$ values and Hill numbers listed in Table 2. The maximum phosphorylation level deduced from the fits was taken as 100%.

Table 2: Apparent Affinities for Ca^{2+} and the Hill Numbers Obtained for the Wild Type and Selected Mutants by Ca^{2+} Titration of Phosphorylation[a]

	25 °C		0 °C	
mutation	$K_{0.5}$ (Ca^{2+}), μM	n_H	$K_{0.5}$ (Ca^{2+}), μM	n_H
wild type	0.39 ± 0.01	1.56 ± 0.05	0.95 ± 0.02	1.90 ± 0.06
Leu249Ala	0.43 ± 0.01	1.79 ± 0.07	ND[b]	ND
Lys252Glu	0.41 ± 0.02	1.95 ± 0.17	2.30 ± 0.11	2.14 ± 0.20
Lys252Arg	0.38 ± 0.02	1.50 ± 0.09	0.75 ± 0.03.	1.86 ± 0.12
Leu253Ala	0.29 ± 0.01	1.98 ± 0.14	ND	ND

[a] Data shown in Figure 8 were analyzed by fitting the Hill equation. [b] ND, not determined.

was found for Leu249Ala, Lys252Glu, and Leu253Ala, but not for Lys252Arg. By computer simulation, we have previously demonstrated that the Hill number should increase toward the limiting value of 2.0 when the rate of Ca^{2+} dissociation from E_1Ca_2 is enhanced and/or the rate of the $E_1PCa_2 \rightarrow E_2P$ transition reduced (*13*). Hence, the observed increase of the Hill number is in accordance with the other findings with these mutants.

For Lys252Glu and Lys252Arg, the Ca^{2+} activation profiles were determined at 0 °C, as well (Figure 8 and Table 2). Under these conditions, the apparent Ca^{2+} affinity of Lys252Glu was reduced 2.4-fold below that of the wild type, indicating that the balance between on- and off-rate was changed relative to wild type when the temperature was reduced. This may be explained by a less steep temperature dependence of the off-rate in the mutant as compared with

the wild type, which would correspond to a lower activation energy associated with Ca^{2+} dissociation in the mutant. This could reflect a more open state of the dissociation pathway in the mutant as compared with the wild type (see Discussion).

DISCUSSION

Roles of Leu249, Lys252, and Leu253 in Control of Ca^{2+} Migration. Of particular interest is the increase of the rate of Ca^{2+} dissociation from the cytoplasmically facing high-affinity binding sites of the E_1Ca_2 form observed for mutants Leu249Ala, Lys252Glu, and Leu253Ala. At pH 6, a 4- to 7-fold increase of the rate of Ca^{2+} dissociation was seen for these mutants, whereas the other mutations exerted much smaller effects (Figure 1 and Table 1). Although Leu253Ala responded less to the pH change than the other mutants and the wild type, the general picture seemed to be the same at pH 7 as at pH 6, with Ca^{2+} dissociation being markedly enhanced in Leu249Ala, Lys252Glu, and Leu253Ala, relative to wild type, and the effects of the other mutations being less pronounced or insignificant (Figure 2). By taking into consideration the rate of phosphorylation of E_1Ca_2 (Figure 3, preincubation in the presence of Ca^{2+}), it is possible to calculate the rate constant for Ca^{2+} dissociation on the basis of the $EP_{ATP+EGTA}/EP_{ATP}$ ratio determined at pH 7 (Figure 2), as previously described (*22*). The resulting rate constants were for the wild type and mutants Leu249Ala, Lys252Glu, and Leu253Ala: 34, 185, 160, and 90 s^{-1}, respectively, corresponding to a 3- to 5-fold increase relative to wild type. Previously, we found that cluster mutation of residues Lys252−Leu−Asp−Glu255 to the residues at the corresponding positions in the Na^+,K^+-ATPase, Glu−Ile−Glu−His, increased the rate of Ca^{2+} dissociation 6-fold at pH 7 (*13*). Hence, the present data clearly demonstrate that also single mutations near the cytoplasmic end of M3 can be effective in increasing Ca^{2+} dissociation, and point to the importance of the specific properties of the side chains at positions 249, 252, and 253. The result obtained for Glu255His (Table 1 and Figure 2) indicates that this mutation is of little importance for the previously observed enhancement of Ca^{2+} dissociation in the cluster mutant. Furthermore, we conclude from the result obtained with Asp254Ala that the negative charge of Asp254 is of little importance for Ca^{2+} migration, although we cannot exclude that the change to the larger glutamate may have contributed to the enhanced rate of Ca^{2+} migration in the cluster mutant.

It is interesting to note that mutations Leu249Ala and Lys252Glu not only increased the rate of dissociation of Ca^{2+} (off-rate), but also increased the on-rate for Ca^{2+}, as evidenced by the similar phosphorylation rates observed for enzyme preincubated with and without Ca^{2+} (Figure 3) as well as by the normal apparent affinity for Ca^{2+} seen by Ca^{2+} titration of steady-state phosphorylation at 25 °C (Figure 8). Furthermore, as shown by the results in Figure 4, in Leu249Ala and Lys252Glu the rate of the Ca^{2+} binding $E_2 \rightarrow E_1Ca_2$ transition was enhanced even at acidic pH, where the release of counter-transported protons is likely to be rate limiting (*24*), thus suggesting an important role for these residues in the control of proton release, as well.

Leu249, Lys252, and Leu253 are not directly involved in Ca^{2+} ligation at the high-affinity membrane sites, as all Ca^{2+} ligands at these sites are provided by oxygen-containing side chains and backbone carbonyls of M4, M5, M6, and M8 (*2*, *4*). Leu249, Lys252, and Leu253 could, however, be associated with the entry pathway for Ca^{2+} and/or be involved in control of the opening and closure of this pathway. The recently published crystal structure of the Ca^{2+}-ATPase in the thapsigargin-bound Ca^{2+}-free form (*12*) provides some clues. In this structure, a water-accessible channel, or pocket, has opened up between M1 and M3 (*12*), see Figure 9A. This channel, which leads to the Ca^{2+} binding residue Glu309 in M4, is closed in the crystal structure of the Ca^{2+}-ATPase in E_1Ca_2 form, where the Ca^{2+} ions presumably are occluded (*4*), and even though the binding of thapsigargin to residues in M3 may have distorted the structure of the Ca^{2+}-free form somewhat in this region, the channel between M1 and M3 may well be closely related to the migration pathway for Ca^{2+}. As shown in Figure 9A, the two hydrophobic side chains of Leu249 and Leu253 form an integral part of the hydrophobic wall lining the channel. The prominent effects on Ca^{2+} migration of substitution of Leu249 and Leu253 with the smaller, but still hydrophobic, alanine may, therefore, result from a destabilization of the wall of the channel, changing channel proportions or allowing the Ca^{2+} ions to dissociate from E_1Ca_2 by an alternative route. The side chains of Asp254 and Glu255 are, on the other hand, more peripherically located with respect to the channel, and this may explain the finding that the negative charges of these side chains are unimportant for Ca^{2+} migration, although some role of the negative charges in directing the Ca^{2+} ions toward the channel entrance might have been expected (*12*).

In the E_1Ca_2 crystal structure, Lys252 is seen to form hydrogen bonds to the two backbone carbonyls of Pro824 and Glu826 in L6−7 (Figure 9B), whereas in the crystal structure of the thapsigargin-bound Ca^{2+}-free form, where the channel is open, the side chain of Lys252 has moved away from L6−7 (Figure 9C). This movement seems to involve the whole M3 helix, which inclines and moves downward toward the lumen (*12*). Simultaneously, M1 moves upward and bends at the suggested channel inlet (Figure 9A), and it can be imagined that the bending occurs as a consequence of steric collision with M3 (*12*). Hence, the movement of M3 could be instrumental in opening the channel. The present finding that the alanine, glutamine, and methionine substitutions of Lys252 and the leucine substitutions of Pro824, Lys825, and Glu826 exerted less functional perturbation than the glutamate substitution of Lys252 shows that the prominent effects of the latter mutation can only be partially accounted for by breakage of the hydrogen bonds to the L6−7 backbone. The presence of the negatively charged glutamate side chain in place of Lys252 must be particularly disturbing. This could possibly be due to electrostatic repulsion of the backbone carbonyls of L6−7 (cf. the energy minimized conformation of the glutamate side chain shown in Figure 9D) or other unfavorable interactions with side chain(s) of L6−7 in the Ca^{2+}-bound form. These effects might destabilize the closed form of the channel by bringing about a movement of M3 resembling to some extent that seen when the two crystal structures of the wild-type enzyme are compared, thus explaining the enhanced rate of dissociation and binding of Ca^{2+} in Lys252Glu.

Importance of Leu253 for the E_1PCa_2 to E_2P Transition and the Function of the Catalytic Site in E_2 and E_2P. Several

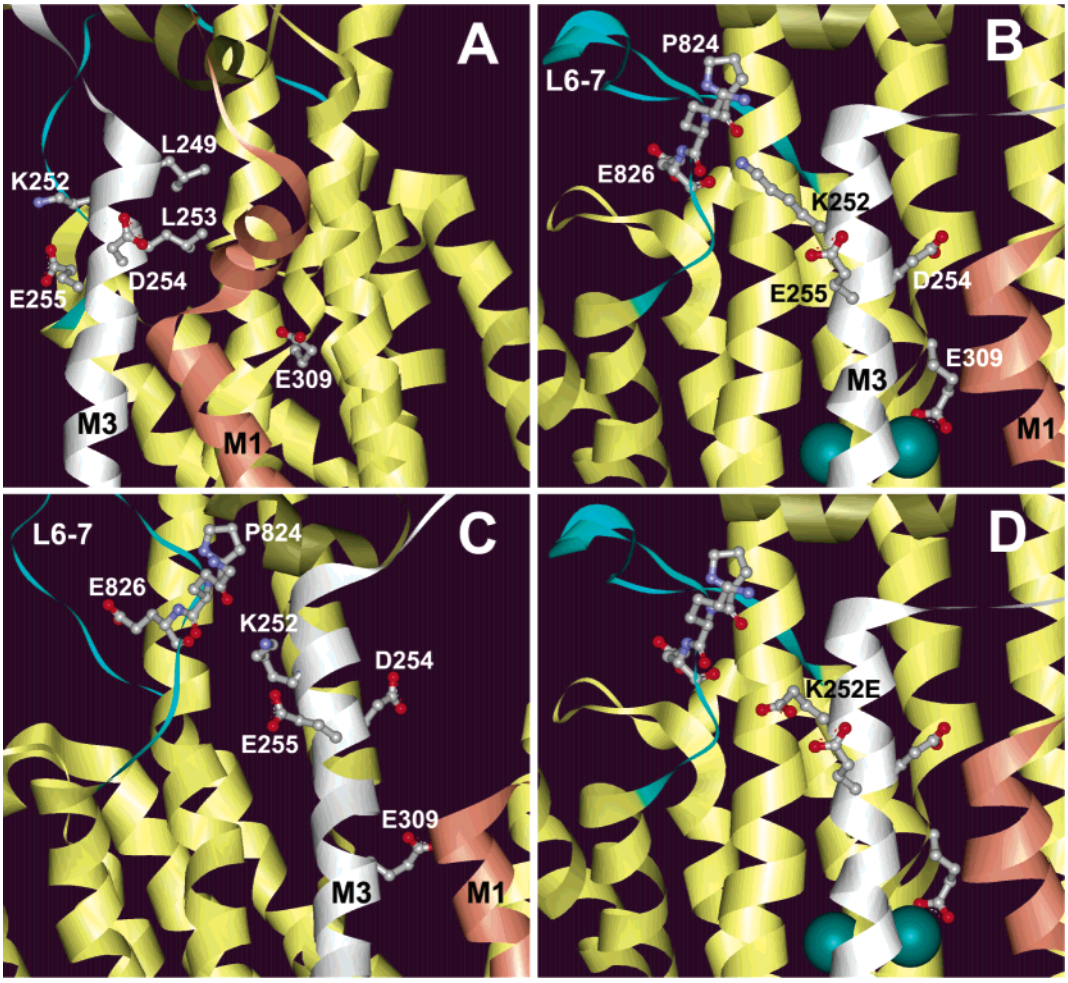

FIGURE 9: Position in the protein structure of residues examined in the present study. The cytoplasmic side is above and the luminal side below. (A) View of the structure of the thapsigargin-bound Ca^{2+}-free form of the Ca^{2+}-ATPase (Protein Data Bank accession code 1IWO). The possible entrance pathway for Ca^{2+} is located between M3 and M1 (bent at the top part) and has its inlet in the upper left part of the figure, with Leu253 and Leu249 forming a hydrophobic lining of the backside. The Ca^{2+} binding residue Glu309 is at the bottom of the pocket. (B) Interaction between Lys252 and backbone carbonyls of L6−7 in the E_1Ca_2 form of the Ca^{2+}-ATPase (Protein Data Bank accession code 1EUL). The view is perpendicular to that corresponding to panel A, and the side chains of Leu253 and Leu249 are now behind the main chain of M3. (C) Position of Lys252 in the thapsigargin-bound Ca^{2+}-free form of the Ca^{2+}-ATPase (Protein Data Bank accession code 1IWO) viewed from the same direction as in panel B. Note that in this conformation Lys252 no longer interacts with L6−7. (D) View of the E_1Ca_2 form identical to that in panel B, but with Lys252 replaced by glutamate (energy minimized conformation of the side chain determined by use of the SWISS-MODEL Comparative Protein Modeling facility (*28*)). Note that the glutamate does not interact with L6−7 in the E_1Ca_2 form. Prepared by use of WebLab Viewer Pro (Molecular Simulations Ltd., Cambridge, England). The Ca^{2+} ions are shown in dark green. The side chains of residues to be highlighted are shown as ball-and-stick. Carbon atoms are shown in grey, nitrogen in blue, and oxygen in red.

lines of evidence have indicated that the actuator domain undergoes large movements in relation to ion translocation (*4*, *6*, *7*), and site-directed mutagenesis and proteolytic cleavage studies have previously demonstrated that the most C-terminal part of the actuator domain, that links it to M3, plays a crucial role for the Ca^{2+}-translocating $E_1PCa_2 \rightarrow E_2P$ conformational transition (*5*, *8*). This suggests that M3 could be a pivotal element in the long-range functional coupling between the catalytic site and the Ca^{2+} binding domain in the membrane. In accordance with this hypothesis, the present results demonstrate that the rate of the $E_1PCa_2 \rightarrow E_2P$ conformational transition is reduced in Lys252Glu, Leu253Ala, and Asp254Ala, to 64, 24, and 40% of the wild type rate, respectively, thus focusing particularly on Leu253 as a critical residue for this conformational transition. Because the $E_1PCa_2 \rightarrow E_2P$ transition is a major rate-limiting step in the wild type pump cycle at saturating substrate concentrations, the rate of this transition should show correlation with the maximum turnover rate for ATPase activity. This was actually observed, as the maximum turnover rate decreased in the order Lys252Glu > Asp254Ala > Leu253Ala (Table 1). Thus, it is not only in relation to Ca^{2+} and thapsigargin binding to dephosphoenzyme, as represented by the two crystal structures, that M3 seems to move. The mutational effects suggest that a movement involving M3 takes place in relation to the Ca^{2+}-translocating $E_1PCa_2 \rightarrow E_2P$ transition of the phosphoenzyme, as well, and that Leu253 is a very important residue in this connection. It should, furthermore, be noted that a slight reduction of the ATP hydrolysis rate with a corresponding slight reduction of the rate of the $E_1PCa_2 \rightarrow E_2P$ transition was seen for Pro824Leu and Glu826Leu, implying some involvement of loop L6−7 in this transition. The putative hydrogen bonds between L6−7 and Lys252 seem to be of limited importance, as the rate of the $E_1PCa_2 \rightarrow E_2P$ transition was wild type-like for all mutants with alterations to Lys252

except Lys252Glu.

An enhanced rate of dephosphorylation of E_2P was found for several M3 mutants. Again, the effect was most pronounced for Leu253Ala (14-fold acceleration relative to wild type), stressing that Leu253 is critical to the long-range communication with the catalytic site. Because Leu253Ala showed the most conspicuous effect, both with respect to the block of the $E_1PCa_2 \rightarrow E_2P$ transition and the enhancement of E_2P hydrolysis, these two changes could be interrelated. In the catalytic site of the E_2P form, the environment of the covalently bound phosphoryl group has changed relative to E_1PCa_2 (*27*), and the three phosphoryl oxygen atoms not involved in covalent bond formation with Asp351 likely interact noncovalently with protein groups, thereby lowering the free energy of hydrolysis relative to the "high-energy" state of the aspartyl phosphate in E_1PCa_2. The enhanced rate of dephosphorylation of E_2P in Leu253Ala may be a consequence of destabilization of the noncovalent part of the phosphoryl−protein interaction in the catalytic site of E_2P imposed from distance. Such a destabilization of E_2P would also slow the $E_1PCa_2 \rightarrow E_2P$ transition.

Leu249Ala, Lys252Glu, and Leu253Ala all displayed much lower apparent affinity for vanadate than the wild type, and again the effect was most pronounced for Leu253Ala. For Leu249Ala and Lys252Glu, that showed an enhanced on-rate for Ca^{2+}, the reduced apparent affinity for vanadate might be ascribed to a shift of the E_2-E_1 conformational equilibrium (reaction 6 in Scheme 1) in favor of the Ca^{2+} binding E_1 state, thus depleting the vanadate-reactive E_2 state. Leu253Ala did, on the other hand, *not* show an increase of the on-rate for Ca^{2+} (Figures 3 and 4), and, yet, the apparent affinity for vanadate was 9-fold reduced relative to wild type. Because vanadate is a phosphoryl transition state analogue that binds at the catalytic site of the E_2 form, the data indicate that in Leu253Ala the catalytic site of E_2 is structurally altered to such an extent that the "true" binding affinity for vanadate is reduced relative to wild type. The same structural change may account for the destabilization of noncovalent phosphoryl−protein interactions in E_2P. In the wild-type enzyme, the catalytic site of the E_2 form is comprised of parts of domain P and domain A, which have moved toward each other, relative to their positions in the E_1Ca_2 form (*6*, *7*, *12*). It is possible that mutation Leu253Ala interferes with the conformational rearrangement that accomplishes the approach of domain A to domain P. This might occur as a consequence of a change in the orientation and relations of M3, as M3 is connected to both domains: to domain A through the peptide backbone and to domain P through a hydrogen bond network involving Glu340 in domain P (*4*).

Comparison with the Na^+,K^+-ATPase. A recent paper has described the functional consequences of mutations to Glu282 in M3 of the closely related Na^+,K^+-ATPase (*29*). Glu282 is located at the position equivalent to Lys252 of the Ca^{2+}-ATPase, and, interestingly, the functional consequences of mutation Glu282Lys in the Na^+,K^+-ATPase were strikingly similar to those of the "inverse" Lys252Glu mutation in the Ca^{2+}-ATPase. Glu282Lys showed an enhanced rate of the $E_2(K_2) \rightarrow E_1Na_3$ transition and a reduced affinity for Na^+, which taken together suggest that the rate of Na^+ dissociation from E_1Na_3 is increased in Glu282Lys (*29*), just as the rate of Ca^{2+} dissociation is increased in the Ca^{2+}-ATPase mutant. Furthermore, the Na^+,K^+-ATPase mutant Glu282Lys showed a block of the $E_1PNa_3 \rightarrow E_2P$ transition and an increased rate of dephosphorylation of E_2P (*29*). Although for the Ca^{2+}-ATPase we found that the corresponding effects on the $E_1PCa_2 \rightarrow E_2P$ transition and dephosphorylation of E_2P were most pronounced for Leu253Ala, they were also seen to some extent for Lys252Glu (Table 1).

ACKNOWLEDGMENT

We thank Karin Kracht and Lene Jacobsen for expert technical assistance, Dr. Bente Vilsen (University of Aarhus) for helpful suggestions, and Dr. R. J. Kaufmann (Genetics Institute, Boston) for the gift of the expression vector pMT2.

REFERENCES

1. de Meis, L., and Vianna, A. L. (1979) *Annu. Rev. Biochem. 48*, 275−292.
2. MacLennan, D. H., Rice, W. J., and Green, N. M. (1997) *J. Biol. Chem. 272*, 28815−28818.
3. Inesi, G., Sumbilla, C., and Kirtley, M. E. (1990) *Physiol. Rev. 70*, 749−760.
4. Toyoshima, C., Nakasato, M., Nomura, H., and Ogawa, H. (2000) *Nature 405*, 647−655.
5. Andersen, J. P., Vilsen, B., Leberer, E., and MacLennan, D. H. (1989) *J. Biol. Chem. 264*, 21018−21023.
6. Patchornik, G., Goldshleger, R., and Karlish, S. J. D. (2000) *Proc. Natl. Acad. Sci. U.S.A. 97*, 11954−11959.
7. Danko, S., Yamasaki, K., Daiho, T., Suzuki, H., and Toyoshima, C. (2001) *FEBS Lett. 505*, 129−135.
8. Møller, J. V., Lenoir, G., Marchand, C., Montigny, C., le Maire, M., Toyoshima, C., Juul, B. S., and Champeil, P. (2002) *J. Biol. Chem. 277*, 38647−38659.
9. Zhang, Z., Lewis, D., Sumbilla, C., Inesi, G., and Toyoshima, C. (2001) *J. Biol. Chem. 276*, 15232−15239.
10. Menguy, T., Corre, F., Juul, B., Bouneau, L., Lafitte, D., Derrick, P. J., Sharma, P. S., Falson, P., Levine, B. A., Møller, J. V., and le Maire, M. (2002) *J. Biol. Chem. 277*, 13016−13028.
11. Nørregaard, A., Vilsen, B., and Andersen, J. P. (1994) *J. Biol. Chem. 269*, 26598−26601.
12. Toyoshima, C., and Nomura, H. (2002) *Nature 418*, 605−611.
13. Andersen, J. P., Sørensen, T. L., Povlsen, K., and Vilsen, B. (2001) *J. Biol. Chem. 276*, 23312−23321.
14. Vilsen, B., Andersen, J. P., Clarke, D. M., and MacLennan, D. H. (1989) *J. Biol. Chem. 264*, 21024−21030.
15. Kaufman, R. J., Davies, M. V., Pathak, V. K., and Hershey, J. W. (1989) *Mol. Cell Biol. 9*, 946−958.
16. Gluzman, Y. (1981) *Cell 23*, 175−182.
17. Chen, C., and Okayama, H. (1987) *Mol. Cell Biol. 7*, 2745−2752.
18. Maruyama, K., and MacLennan, D. H. (1988) *Proc. Natl. Acad. Sci. U.S.A. 85*, 3314−3318.
19. Vilsen, B., Andersen, J. P., and MacLennan, D. H. (1991) *J. Biol. Chem. 266*, 16157−16164.
20. Sørensen, T., Vilsen, B., and Andersen, J. P. (1997) *J. Biol. Chem. 272*, 30244−30253.
21. Baginski, E. S., Foa, P. P., and Zak, B. (1967) *Clin. Chem. 13*, 326−332.
22. Sørensen, T. L., Dupont, Y., Vilsen, B., and Andersen, J. P. (2000) *J. Biol. Chem. 275*, 5400−5408.
23. Petithory, J. R., and Jencks, W. P. (1988) *Biochemistry 27*, 5553−5564.
24. Forge, V., Mintz, E., and Guillain, F. (1993) *J. Biol. Chem. 268*, 10961−10968.
25. Cantley, L. C., Jr., Cantley, L. G., and Josephson, L. (1978) *J. Biol. Chem. 253*, 7361−7368.
26. Pick, U. (1982) *J. Biol. Chem. 257*, 6111−6119.
27. de Meis, L., Martins, O. B., and Alves, E. W. (1980) *Biochemistry 19*, 4252−4261.
28. Guex, N., and Peitsch, M. C. (1997) *Electrophoresis 18*, 2714−2723.
29. Toustrup-Jensen, M., and Vilsen, B. (2002) *J. Biol. Chem. 277*, 38607−38617.

BI0271897